



Cite this: DOI: 10.1039/c9pp00010k

2-Azo-, 2-diazocine-thiazols and 2-azo-imidazoles as photoswitchable kinase inhibitors: limitations and pitfalls of the photoswitchable inhibitor approach†

Miriam Schehr,^a Chiara Ianes,^b Jörn Weisner,^c Linda Heintze,^d Matthias P. Müller,^e Christian Pichlo,^e Julia Charl,^e Elena Brunstein,^e Julia Ewert,^a Marc Lehr,^a Ulrich Baumann,^e Daniel Rauh,^c Uwe Knippschild,^b Christian Peifer^{*d} and Rainer Herges^{*a}

In photopharmacology, photoswitchable compounds including azobenzene or other diarylazo moieties exhibit bioactivity against a target protein typically in the slender *E*-configuration, whereas the rather bulky *Z*-configuration usually is pharmacologically less potent. Herein we report the design, synthesis and photochemical/inhibitory characterization of new photoswitchable kinase inhibitors targeting p38 α MAPK and CK1 δ . A well characterized inhibitor scaffold was used to attach arylazo- and diazocine moieties. When the isolated isomers, or the photostationary state (PSS) of isomers, were tested in commonly used *in vitro* kinase assays, however, only small differences in activity were observed. X-ray analyses of ligand-bound p38 α MAPK and CK1 δ complexes revealed dynamic conformational adaptations of the protein with respect to both isomers. More importantly, irreversible reduction of the azo group to the corresponding hydrazine was observed. Independent experiments revealed that reducing agents such as DTT (dithiothreitol) and GSH (glutathione) that are typically used for protein stabilization in biological assays were responsible. Two further sources of error are the concentration dependence of the *E*-*Z*-switching efficiency and artefacts due to incomplete exclusion of light during testing. Our findings may also apply to a number of previously investigated azobenzene-based photoswitchable inhibitors.

Received 7th January 2019,
Accepted 21st March 2019

DOI: 10.1039/c9pp00010k

rsc.li/pps

Introduction

Photoswitchable molecules which undergo conformational or configurational changes triggered by light show great potential in versatile applications such as molecular machines,^{1–3} controlling conductivity,^{4,5} or pharmacology.^{6–9} Especially utilization of photoswitchable moieties in pharmacologically active

compounds, namely photopharmacology, is a rapidly evolving field with great potential. The goal is to control the activity of molecules by changing their geometry and thus their bioactivity using light as a non-invasive trigger. This approach opens the possibility of a spatially and temporally controlled drug therapy. Furthermore, fundamental biological processes can be precisely studied using photoresponsive pharmacological tools. Following this strategy, a number of photoswitchable molecules for different targets and pharmacological purposes have been developed in academia. A selection of examples is presented in Table 1. Mostly, azobenzene moieties were used as the *E/Z*-photoswitchable units allowing for rather large steric changes of the respective pharmacophore. Thus, for smartly designed and optimized inhibitors one could ideally expect one isomer to be biologically highly active against a specific target, whereas the other isomer should show no activity at all. At least, both isomers should exhibit significantly different activities. Typically, for azobenzenes, the *E*-isomer has a higher biological activity in comparison to the *Z*-isomer. However, frequently the difference in biological activity is rather small. Examples of efficient azobenzene based

^aOtto Diels-Institute of Organic Chemistry, Christian Albrechts University Kiel, Otto-Hahn-Platz 4, 24118 Kiel, Germany. E-mail: rherges@oc.uni-kiel.de

^bDepartment of General and Visceral Surgery, Ulm University Hospital, Albert-Einstein-Allee 23, 89081 Ulm, Germany

^cFaculty of Chemistry and Chemical Biology, TU Dortmund University and Drug Discovery Hub Dortmund (DDHD) am Zentrum für integrierte Wirkstoffforschung (ZIW), Otto-Hahn-Straße 4a, 44227 Dortmund, Germany

^dInstitute of Pharmacy, Christian Albrechts University Kiel, Gutenbergstraße 76, 24118 Kiel, Germany. E-mail: cpeifer@pharmazie.uni-kiel.de

^eDepartment of Chemistry, University of Cologne, Otto-Fischer-Straße 12-14, 50674 Cologne, Germany

† Electronic supplementary information (ESI) available. CCDC 1885848. For ESI and crystallographic data in CIF or other electronic format see DOI: 10.1039/c9pp00010k

Table 1 IC₅₀ values of the different isoforms and the corresponding factor of selected photoswitchable biomolecules published by different groups

Study	Selected target	Photoswitchable moiety	IC ₅₀ value (<i>E/trans</i> or open)	IC ₅₀ value (<i>Z/cis</i> or closed)	Ratio
Morton <i>et al.</i> ¹⁴	Cysteine protease calpain	Azobenzene	45 nM	175 nM	3.8-fold
König <i>et al.</i> ¹¹	Human carbonic anhydrase I	Diarylethene	8 nM	400 nM	50-fold
König <i>et al.</i> ¹⁵	Histone deacetylase	Diarylmaleimide	4.2 μM	92.3 μM	22-fold
Feringa <i>et al.</i> ¹⁶	Proteasome	Azobenzene	41 nM	91 nM	2-fold
Feringa <i>et al.</i> ¹⁰	Histone deacetylase	Azobenzene	21.7 μM	0.56 μM	39-fold
Fuchter <i>et al.</i> ¹⁷	Amidohydrolase	Azobenzene	2.5 μM	0.18 μM	14-fold
König <i>et al.</i> ¹⁸	Histone deacetylase	Dithienylethene	18 μM	4.5 M	4-fold
König <i>et al.</i> ¹⁹	Histone deacetylase	Fulgimides	29.6 μM	19.9 μM	1.5-fold
Grötli <i>et al.</i> ¹²	RET kinase	Azobenzene	150 nM	580 nM	4-fold
Branda <i>et al.</i> ²⁰	Protein kinase C	Diarylethene	580 nM	inactive	—
Liskamp <i>et al.</i> ¹³	Spleen tyrosine kinase	Azobenzene	65 nM (<i>K_D</i> value)	146 nM (<i>K_D</i> value)	11-fold

photoswitchable inhibitors include a histone deacetylase studied by Feringa *et al.*¹⁰ where a 39-fold difference between the *E*- and the *Z*-isomer was observed. Comparably, König *et al.*¹¹ were able to achieve a 50-fold difference in activity of a carbonic anhydrase using the open or closed form of a diarylethene as a photoswitch. Regarding various targets of photoswitchable inhibitors, only few protein kinase inhibitors based on azobenzenes were reported, including examples of Grötli *et al.*¹² (*E/Z*: 4-fold), and Liskamp *et al.*¹³ (*E/Z*: 11-fold).

Protein kinases are phosphotransferases that catalyse the transfer of the γ -phosphate group from ATP to a hydroxyl group of substrates. They play important roles in signal transduction cascades regulating different cellular processes like cell differentiation, cell proliferation or apoptosis. Thus, dysregulation of key protein kinases often leads to severe disorders like cancer, inflammation, or neurodegenerative diseases.^{21–25} The human kinome consists of more than 500 different protein kinases, rendering selectivity of an inhibitor for a specific kinase a key issue. Until today, more than 40 approved protein kinase inhibitors are used in therapy, mostly for cancer treatment.^{26–28} In this context, photoswitchable kinase inhibitors allowing spatial and temporal control by light would offer great therapeutical advantages. Such an inhibitor could be specifically activated on a focussed site of action, which may lead to high efficacy and reduced systemic side effects. Motivated by the relatively few examples of photoswitchable protein kinase inhibitors reported so far, we started to investigate the applicability of photoswitches towards this compound class in more detail.

In the present study we report on the design, synthesis and biological evaluation of photoswitchable inhibitors for p38 α Mitogen-activated Protein Kinase (p38 α MAPK) and the highly related Casein Kinase 1 δ (CK1 δ). As model compound we used the known 4,5-diarylimidazole compound **1** which is a highly potent inhibitor of both p38 α MAPK and CK1 δ .²⁹ Structural data for **1** in the ATP binding pocket and detailed structure-activity relationships (SAR) for CK1 δ were available and provided the basis for a rational design strategy of the photoswitchable inhibitors (Fig. 1).²⁹ Preliminary docking studies revealed the methylthioether substituted 2-imidazole position in **1** as the most suitable position to attach the switchable azo

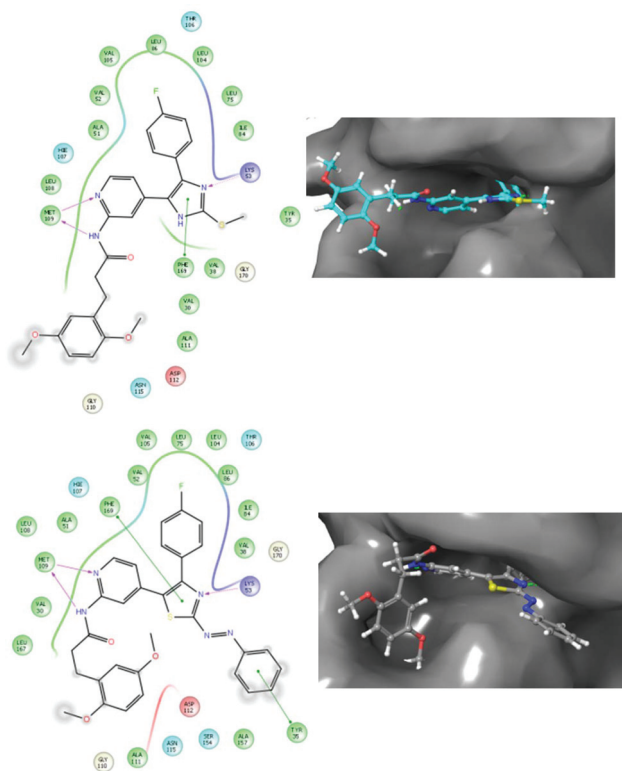


Fig. 1 Top: 2D ligand-interaction diagram (LID) and corresponding 3D binding mode showing the protein surface of original ligand **1** (turquoise) in the ATP active site of p38 α MAPK as determined by X-ray crystallography (pdb 5ML5).²⁹ Bottom: LID and 3D binding mode of designed photoswitchable azo-compound **2** in the ATP active site of p38 α MAPK based on docking calculations. The ligand reveals a plausible binding mode only in the *E*-configuration, whereas the *Z*-configured ligand did not adequately fit into the ATP pocket due to significant steric clashes. Similar results were obtained for designed ligand **3** in p38 α MAPK, and for **2** and **3** in the highly related structure of CK1 δ (pdb 5MQV, not shown). For details see ESI.†

unit. The heterocyclic, aromatic five-ring was included as part of the switching diarylazo system (Fig. 1). Azobenzene-type photoswitches with one of the benzene rings replaced by a 5-membered heterocyclic ring often exhibit favourable photo-

physical properties,³⁰ however, *Z*-1*H*-azoimidazoles rapidly isomerize back to the more stable *Z*-isomer *via* tautomeric structures.³¹ Therefore, the imidazole unit must be *N*-methylated, or the imidazole has to be replaced by *e.g.* a thiazole ring (Fig. 1, bottom) to obtain a system with a sufficient half-life in the *Z*-configuration.

According to the crystallographically determined binding mode of **1** in p38 α MAPK,²⁹ this moiety is situated in a narrow channel formed by Tyr35, Val38, Lys53, Glu71 and Phe169 (amongst further residues) in close proximity to the crucial activation loop and the glycine-rich loop. Therefore, this pocket of the protein kinase should be able to accommodate the azoaryl moiety in *E*-configuration, but not in *Z*-configuration, thus translating into different photoresponsive bioactivities, respectively. Furthermore, we extended this concept by a thiodiazocine moiety attached to the thiazole core in a similar manner (Fig. 2). The diazocine moiety was chosen because this class of compounds has photochemical properties that are highly favorable for photoswitchable ligand design. Compared to azobenzenes, diazocines are thermodynamically more stable in the *Z*-configuration and can be switched to the metastable *E*-configuration upon irradiation (see Scheme 1).³²

In docking studies, the metastable *E*-configuration of **4** was calculated to fit more precisely into the binding pocket than

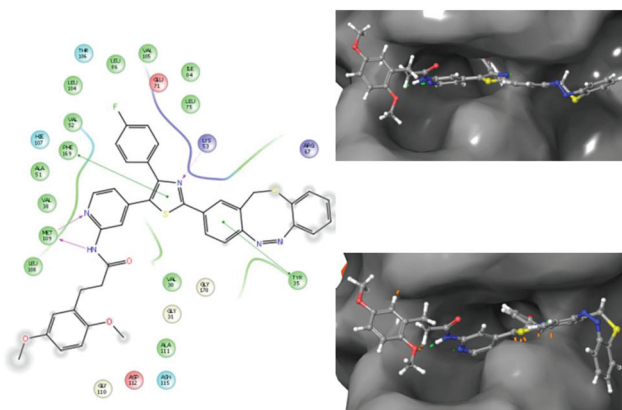


Fig. 2 Top: Calculated 2D ligand-interaction diagram (LID) and 3D binding mode showing the protein surface of designed ligand **4** (*E*-configuration) within the ATP active site of p38 α MAPK (pdb 5ML5²⁹) determined by docking. Bottom: Distorted suboptimal binding pose of compound **4** in the *Z*-configuration causing steric clashes (dotted orange lines). For details see ESI.†



Scheme 1 The diazocine moiety is thermodynamically more stable in the *Z*-configuration and can be converted to the metastable *E*-configuration upon irradiation with 405 nm.

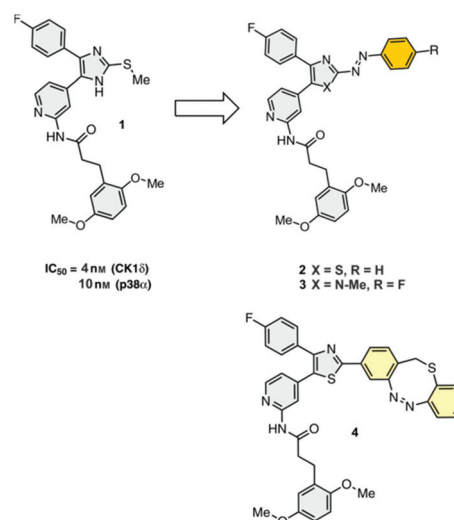
the thermodynamically stable *Z*-configuration of **4**. Consequently, a higher bioactivity of the metastable *E*-configuration is expected.

Results and discussion

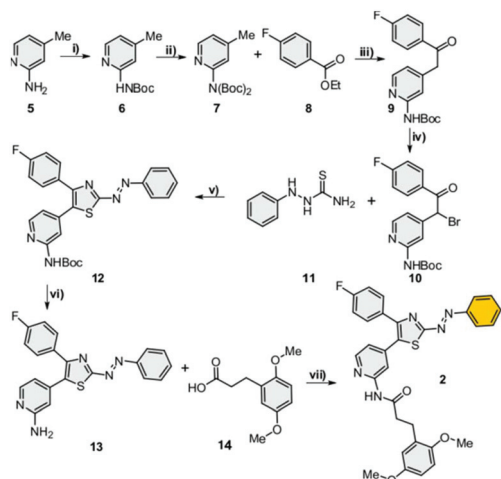
Synthesis and photophysical properties

Based on the design concept of the photoswitchable p38 α MAPK inhibitor outlined above, we aimed at the synthesis and photochemical/photophysical characterization of target compounds **2–4** (summarized in Scheme 2).

Our straightforward seven-step synthesis of 2-azo-thiazole inhibitor **2** is presented in Scheme 3 (for detailed synthetic procedures see ESI†). Starting material 2-amino-4-methylpyridine **5** was successively double Boc-protected with di-*tert*-butyl dicarbonate at first in *tert*-butanol and then using 4-dimethylaminopyridine (DMAP) in THF at room temperature.³³ Attempts of direct double protection always led to a mixture of single and double Boc-protected products **6** and **7**. The double protection, however, is necessary for the synthesis of the ethanone derivative **9**. Here, the methyl group was deprotonated with sodium hexamethyldisilazane (NaHMDS) in THF and reacted with ethyl-4-fluorobenzoate **8** to obtain the ethanone derivative **9**.³⁴ During this reaction, one of the Boc-groups is cleaved. Using the single Boc-protected methylpyridine **6** for the formation of ethanone **9** led to complete decomposition of the starting material **6**. After NBS bromination of the ethanone in the α -position, the obtained α -bromoketone **10** was reacted with thiosemicarbazide **11** to form the thiazole ring functionalized with a hydrazine moiety. The hydrazine could be selectively oxidized *in situ* by bubbling compressed air through the



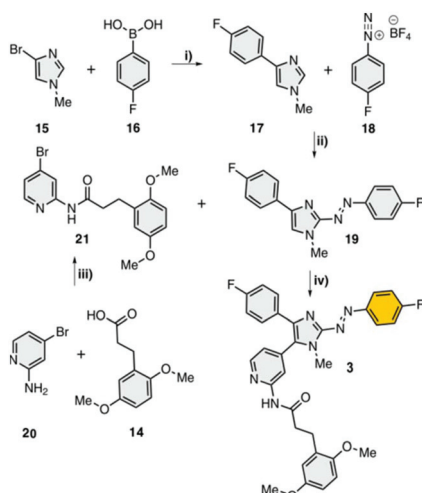
Scheme 2 Potential photoswitchable target inhibitors **2–4** derived from the known CK1 δ /p38 α MAPK inhibitor **1**.²⁹ In target structure **2** and **3** the 1*H*-imidazole is replaced by 1,3-thiazole or 1-methyl imidazole and the thiomethyl substituent is replaced by an azophenyl group. In target inhibitor **4** a photoswitchable *S*-diazocine unit is attached to the 2-position of the 1,3-thiazole.



Scheme 3 Reaction conditions: (i) Boc anhydride, *t*-butanol, 30 °C, 68%; (ii) Boc anhydride, THF, 99%; (iii) NaHMDS, THF, 0 °C, 60%; (iv) NBS, AcOH/DCM, 97%; (v) AcOH, compressed air, THF, 80 °C, 42%; (vi) HCl, ethyl acetate, 55 °C, 97%; (vii) T3P® (propylphosphonic anhydride), DIPEA, 95 °C, 48%.

solution yielding the azobenzene moiety **12**.³⁵ Deprotection of the 2-aminopyridine **12** with hydrochloric acid led to the amine **13**, which was functionalized with the 3-(2,5-dimethoxyphenyl)propionic acid **14** *via* peptide coupling conditions to afford target compound **2**.³⁶

The 2-azo-imidazole inhibitor **3** was obtained by a four-step synthesis (Scheme 4). In the first synthetic step, the 4-fluorophenyl moiety **17** was introduced *via* Suzuki cross coupling of 4-fluorophenylboronic acid **16** and 4-bromo-1-methyl-1*H*-imidazole **15**.³⁷ In the next step, to afford the 2-azoimidazole **19**, the imidazole 2-position was lithiated with *n*-butyllithium and reacted with 4-fluorotetrafluorodiazonium salt **18**, which was



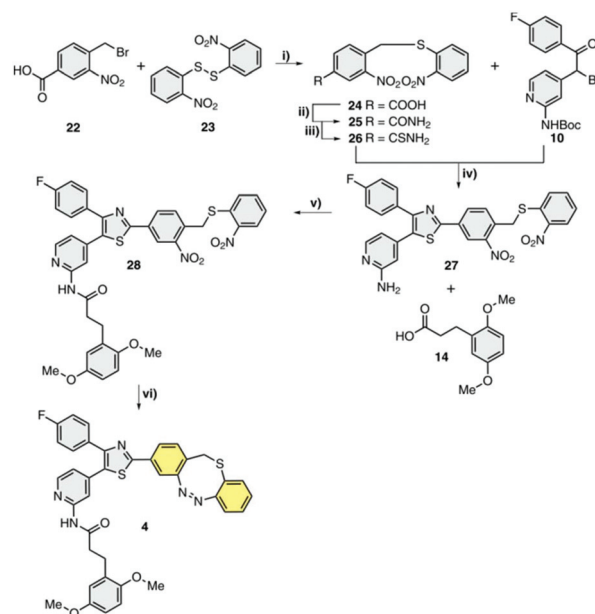
Scheme 4 Reaction conditions: (i) Pd[dppf]Cl₂, BnNEt₃Cl, CsF, toluene/water, 90 °C, 84%; (ii) *n*-BuLi, THF, -78 °C, 19%; (iii) T3P®, DIPEA, ethyl acetate, 95 °C, 57%; (iv) Pd(OAc)₂, K₂CO₃, DMAc, 150 °C, 18%.

prepared according to literature.^{38,39} In the last synthesis step the pyridine moiety functionalized *via* peptide coupling with 3-(2,5-dimethoxyphenyl)propionic acid **14** was introduced in the azoimidazole **19** using palladium catalyzed conditions to afford target compound **3**.⁴⁰

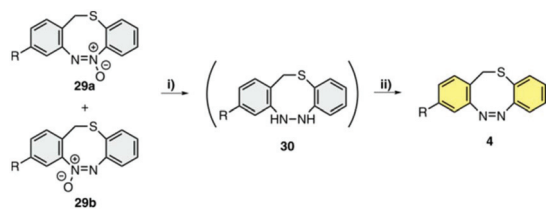
To obtain the 2-diazocine-thiazole **4**, the synthetic route was started with the synthesis of the functionalized diazocine precursor **26** (Scheme 5).

Disulfide **23** was reduced with sodium borohydride and then reacted *in situ* with the functionalized benzyl bromide **22** to afford thioether **24**.⁴¹ The carboxylic acid was converted to the acid amide **25**, which could further be functionalized with Lawesson's reagent to yield thioamide **26**.⁴² In the next step, the thioamide functionalized diazocine precursor **26** was used in a ring closing reaction with α -bromoketone **10** forming the thiazole compound **27**. After peptide coupling with 3-(2,5-dimethoxyphenyl)propionic acid **14** followed by reductive azo condensation with lead, a small portion of the desired diazocine **4** could be isolated directly.⁴³ The majority of the product however was a mixture of azoxy compounds **29a/29b** (Scheme 6). The latter mixture was converted to the diazocine **4** without further purification by another two-step procedure. The non-defined mixture of **29a/29b** was reduced with lead powder using high power ultrasound conditions to yield hydrazine **30**. Hydrazine **30** was then oxidized by copper(II)chloride in a methanolic sodium hydroxide solution to again give the target diazocine **4**.

Using these combined techniques, the 2-diazocine-thiazol **4** could be obtained with a total yield of 12%.



Scheme 5 Reaction conditions: (i) NaBH₄, THF, 60 °C, 35%; (ii) 1. Oxalyl chloride, 2. aq. ammonia, ethyl acetate, quant. (iii) Lawesson's reagent, THF, 80 °C, 78%; (iv) 1. MeCN, 2. AcOH/HCl, 80 °C, 36%; (v) T3P®, DIPEA, 95 °C, ethyl acetate, 37%; (vi) 1. Pb, NEt₃/formic acid/MeOH/H₂O, 2. Cu(I)Cl, NaOH in MeOH, compressed air, 12%.



Scheme 6 Reaction conditions: (i) Pb, NEt₃/formic acid/MeOH/H₂O, high power ultrasound; (ii) Cu(II)Cl₂, NaOH in MeOH, compressed air.

The photochemical properties of key compounds 2–4 were investigated using UV/vis and ¹H NMR spectroscopy. Unfortunately, besides poor solubility in water, compounds 2–4 showed in aqueous medium very poor photochemical properties. Since an adequate photochemical characterization was not possible in aqueous solutions, we performed the photochemical analysis in DMSO solution. In Fig. 3, UV/vis spectra of the 2-azo-thiazole 2 and -imidazole 3 including photostability tests are shown. The 2-azo-thiazole 2 in the *E*-configuration (black line) displays absorption maxima at $\lambda_{\text{max}} = 294$ nm and $\lambda_{\text{max}} = 417$ nm. After irradiation with 435 nm the $\pi\pi^*$ band decreases significantly until the photostationary state (PSS) between the *E*- and the *Z*-isomer (red line) is reached, with absorption maxima at 289 nm and 376 nm, respectively. To trigger the reverse isomerisation (*Z* towards *E*), irradiation into the $\pi\pi^*$ band of the *Z*-isomer with 525 nm was used (Fig. 3, top left, blue line). Due to an overlap of the $\pi\pi^*$ band of the *E*-isomer and the $\pi\pi^*$ band of the *Z*-isomer, back isomerization could not be achieved quantitatively (Fig. 3, blue line). The UV/vis spectra of the 2-azo-imidazole 3 are similar to those of compound 2. For the *E*-isomer, absorption maxima at $\lambda_{\text{max}} =$

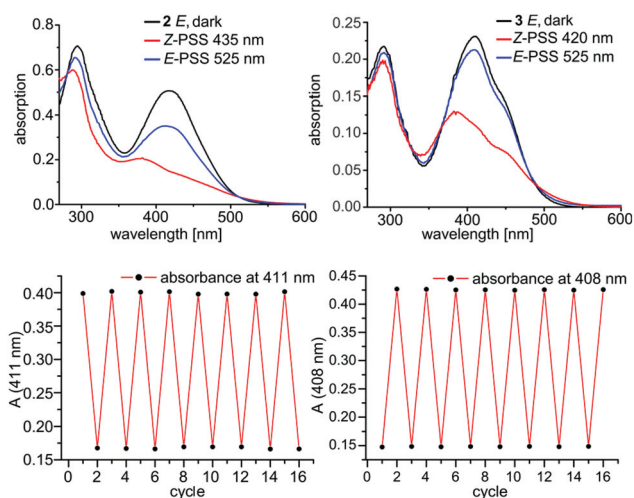


Fig. 3 Top: UV spectra of 2-azo-thiazole 2 (50 μM, DMSO, left) and 2-azo-imidazole 3 (10 μM, DMSO, right). The spectra of the *E*-isomers are plotted in black and the PSS spectra measured after irradiation with 435/420 nm are plotted in red. The PSS of back isomerization with 525 nm is plotted in blue. Bottom: Absorbance of 2-azo-thiazole 2 (DMSO, 411 nm, left) and 2-azo-imidazole 3 (DMSO, 408 nm right) upon irradiation with 435/420 nm and 525 nm in an alternating sequence.

291 nm and $\lambda_{\text{max}} = 408$ nm ($\pi\pi^*$) with a slight shoulder at 450 nm were observed (black line). Irradiation of this species with 420 nm gives the PSS containing both, *E*- and *Z*-configurations (red line) with absorption maxima at $\lambda_{\text{max}} = 290$ nm, $\lambda_{\text{max}} = 375$ nm and $\lambda_{\text{max}} = 450$ nm. Again, reverse isomerization can also be initiated by irradiation of the $\pi\pi^*$ band with light of 525 nm and, similar to compound 2, the back isomerization cannot be achieved quantitatively (Fig. 3, top right, blue line). However, both compounds 2 and 3 show excellent photostability in DMSO when repeatedly photoswitched between the *E*- and *Z*-configuration, respectively (Fig. 3, bottom).

The UV absorption of the diazocine moiety of 2-diazocine-thiazole 4 is relatively weak compared to the UV absorption of the residual molecule. Therefore, only the visible absorption of the diazocine (420–700 nm) is displayed in Fig. 4 (for complete UV/vis spectrum see ESI†). The UV spectrum of the *Z*-isomer of 4 is plotted in black. Upon irradiation with 405 nm the $\pi\pi^*$ band of the diazocine moiety in the *E*-configuration with $\lambda_{\text{max}} = 520$ nm emerges (Fig. 4, red line). Back isomerization can be achieved using 525 nm quantitatively. Similar to the switchable inhibitors 2 and 3, compound 4 shows excellent photostability in solution when subjected to repeated irradiation with 405 and 525 nm in an alternating sequence (Fig. 4).

Photostationary states and half-lives ($t_{1/2}$) of the respective *E/Z*-isomers were measured using either ¹H NMR or UV/vis spectroscopy in deuterated DMSO. The results obtained for compounds 2–4 are summarized in Table 2.

Although the UV/vis spectra of 2-azo-thiazole 2 show a satisfying *E*-to *Z*-conversion of estimated more than 80%, NMR analysis at higher concentrations (3.52 mM) indicates a considerably lower conversion to the *Z*-isomer (29%). At even higher concentrations, (17.6 mM) NMR analysis indicates no photochemical *E* to *Z* conversion of 2. Back isomerization with 525 nm shows concentration dependence: NMR analysis indicated just a small *Z* to *E* conversion of 10%. Interestingly, concentration dependence of heteroazo compounds affected the half-life rather than the photostationary states (also reported in literature).^{44,45} We attribute the concentration dependent switching behaviour to self-quenching effects and the formation of agglomerates. In line with this notion, examination of highly diluted solutions (5 μM–100 μM) by UV/vis spectroscopy showed no concentration dependency. This concen-

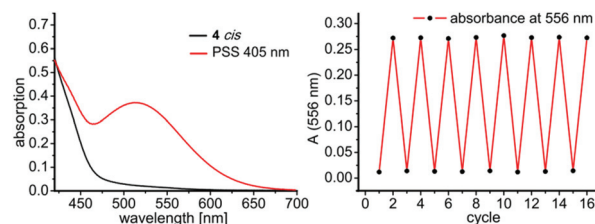


Fig. 4 Left: UV spectra of 2-diazocine-thiazole 4 (290 μM, DMSO). The *Z*-spectrum is plotted in black and the PSS spectrum measured after irradiation with 405 nm is plotted in red. Right: Absorbances of 2-diazocine-thiazole 4 (DMSO, 556 nm) after alternating irradiation at 405 nm and 525 nm in repeated switching cycles.

Table 2 Photostationary states (PSS) and half-lives ($t_{1/2}$) of compound 2–4 measured in deuterated DMSO at 27 °C

Compound	Isomer: PSS (λ)	PSS (525 nm)	$t_{1/2}$
2	Z: 29% (435 nm)	E: 81%	13 min ^a
3	Z: 85% (420 nm)	E: 88%	2.4 h
4	E: 47% (405 nm)	Z: 100%	3.2 d

^a Determined using UV/vis spectroscopy.

tration dependent switching behaviour of 2-azo-thiazol 2 has to be further investigated. However, we conclude that the *E* to *Z* conversion at the very low (μ M) concentrations employed in biological assays, are not hampered by aggregation effects. The half-life of 13 min of *E*-2-azo-thiazole 2, however, is probably too short in terms of common enzymatic assays. In contrast, 2-azo-imidazole 3 has promising photophysical properties with a *E* to *Z* conversion of 85% and a half-life of 2.4 hours. The diazocine functionalized thiazole 4 shows a *Z* to *E* conversion of 47% with a rather long half-life of 3.2 days. In contrast to compound 2, compound 3 and 4 showed no concentration dependent photostationary states.

Determination of IC₅₀ values

Having photoswitchable compounds 2–4 as isolated isomers, or photostationary mixtures, in hand, we set out for enzymatic evaluation of the inhibition of p38 α MAPK and the structurally highly related CK1 δ . In order to switch towards the photostationary states, the DMSO compound stock solutions were irradiated with appropriate wavelengths (Fig. 3 and 4) prior to dilution with water. However, in the actual *in vitro* kinase assays the situation was not as clear as expected. Compounds 2 and 3 in both the *E*- and *Z*-configuration were determined to be highly potent inhibitors with IC₅₀ values in the nM range (Table 3) which is in sharp contrast to the design concept and modelling results. In comparison, 4 showed no significant inhibition in both configurations up to a concentration of 10 μ M. Strikingly and in contrast to our *E*-active/*Z*-less-active hypothesis, in the regular p38 α MAPK and CK1 δ assays under controlled light conditions or in the dark, compound 2 was even more active when the *Z*-isomer was enriched *via* photoisomerization. To elucidate this discrepancy and to characterize

the mode of binding in the active site on a molecular level, we aimed at X-ray crystallographic analyses of ligand–protein complexes.

X-ray crystallographic analysis of photoswitchable ligand-p38 α MAPK and -CK1 δ complexes

p38 α . Compound 2 was co-crystallized in complex with p38 α MAPK under ambient lab conditions and the structure was solved by molecular replacement (Fig. 5). Within the structure, however, a conformation of the diarylazo moiety was observed that was neither compatible with the expected angles of the *E*- nor the *Z*-configuration. In fact, the reduced hydrazine 31 was present, forming an additional H-bond with Gly170. Within the crystallization solution, dithiothreitol (DTT) was used to avoid oxidation of the protein. Reducing agents such as DTT and glutathione (GSH) are known to have the reducing strength to reduce some azo moieties.^{46–48} Thus, we hypothesized DTT to be the responsible agent for the reduction of the diarylazo moiety. To confirm this experimentally, we used a 3.5 nM solution of compound 2 in a NMR tube, added 3 mM solution of DTT in DMSO and investigated the reaction progress by ¹H NMR spectroscopy. After addition of the DTT solution, a second set of signals immediately emerged providing evidence for the formation of the hydrazine derivative 31. Furthermore, when a large excess of DTT was used, the signals of 2 completely vanished to quantitatively yield the hydrazine derivative 31. Additionally, high resolution mass spectrometry confirmed the formation of the hydrazine derivative 31 and kinetic measurements *via* UV/vis spectroscopy additionally revealed a very short half-life of 3 min for the reduction (see ESI†).

Similar to DTT for p38 α assays and crystallization, GSH (glutathione) as reducing/protein stabilizing agent is deployed in the regular setup of the CK1 δ assays. In contrast to the above described NMR experiments with DTT, we were not able to prove the reduction of compound 2 with GSH. However, by using a large excess of GSH respective changes could be detected in UV/vis spectra. From other studies it is reported that *Z*-azo compounds were reduced up to 100-times faster than the corresponding *E*-azo compounds.⁴⁹ In line with these data, in our study the assays enriched in the *Z*-isomer contain far more hydrazine 31, which could also provide an explanation for the apparent higher inhibitory activity of the

Table 3 Biological activities of inhibitors 2–4. IC₅₀ values were determined ($n = 3$) for the isolated *E*-isomers, and for the *E/Z*-PSS's at respective irradiation wavelengths (in parentheses). Abbreviations: n.a. not active up to 10 μ M inhibitor concentration, PSS: photostationary state

Compound	Isomer Irradiation Wavelength	CK1 δ		p38 α	
		IC ₅₀ \pm SD/nM	Maximal inhibition (bottom plateau) \pm SD/% residual kinase activity	IC ₅₀ \pm SD/nM	Maximal inhibition (bottom plateau) \pm SD/% residual kinase activity
2	<i>E</i> (dark)	147 \pm 38.3 nM	37.9 \pm 0.95	29.1 \pm 8.62 nM	4.09 \pm 3.45
	PSS (435 nm)	54.7 \pm 9.70 nM	5.40 \pm 0.25	2.36 \pm 0.61 nM	–1.75 \pm 2.62
3	<i>E</i> (dark)	138 \pm 26.5 nM	23.0 \pm 0.48	83.2 \pm 8.68 nM	1.91 \pm 5.24
	PSS (420 nm)	218 \pm 2.33 nM	22.4 \pm 5.00	115 \pm 28.9 nM	8.24 \pm 2.38
4	<i>Z</i> (dark)	n.a.	—	n.a.	—
	PSS (405 nm)	n.a.	—	n.a.	—

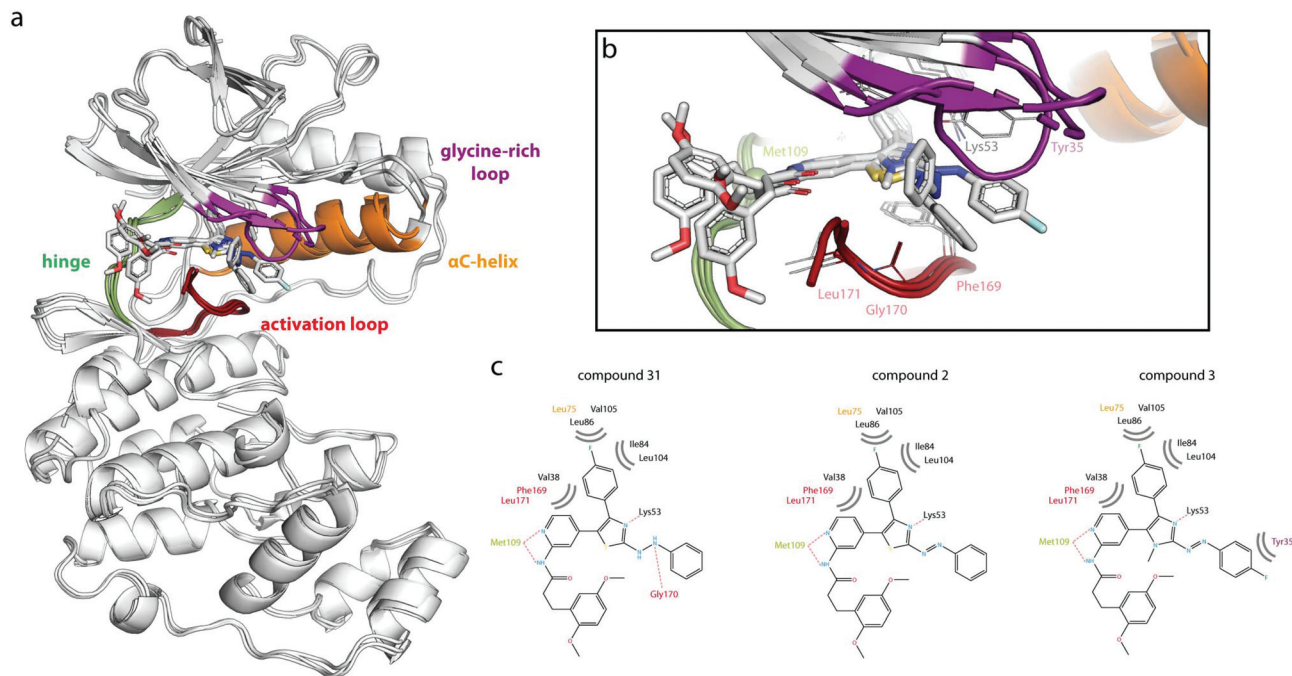


Fig. 5 Crystal structure of p38 α MAPK in complex with compound 2 and 3. (a) Overview of the kinase domain including the binding pocket and important regions (hinge region – green, glycine-rich loop – magenta, α C-helix – orange, activation loop – red). (b) Zoom of the binding pocket highlighting the differences of the mode of binding of compound 2 (and the reduced hydrazine compound 31) and compound 3. The core of the molecules always binds in a similar orientation, whereas differences can be observed within the diarylazo moiety and the proximal glycine-rich loop. The solvent exposed 2,5-dimethoxyphenyl-group is not well resolved in the structures and is modelled in different conformations. (c) Most interactions of the compounds 2, 3 and 31 are similar in the different structures and mostly of hydrophobic nature. Observed differences included an additional interaction of the hydrazine of compound 31 and the carbonyl of Gly170 as well as an additional stacking interaction of the fluorophenyl group of compound 3 and Tyr35 (glycine-rich loop).

Table 4 Measured IC₅₀ values of photoswitchable inhibitor 2 with p38 α in the absence of DTT. IC₅₀ values were determined ($n = 3$) for the isolated *E*-isomer, and for the *E/Z*-PSS after irradiation with 435 nm

Compound 2	IC ₅₀ \pm SD/nM	Maximal inhibition (bottom plateau) \pm SD/% residual kinase activity
Dark (<i>E</i>)	67.5 \pm 23.7	46.6 \pm 1.54
PSS (435 nm)	105 \pm 34.4	9.98 \pm 3.71

assumed *Z*-isomer (in fact being hydrazine 31). This leads to the conclusion that the most inhibitory active compound is neither the *E*- nor *Z*-isomer of 2 but rather the hydrazine compound 31. This hypothesis was verified by repetition of the p38 α *in vitro* kinase assay in the absence of DTT (Table 4). Herein, the IC₅₀ values for both the *E*-isomer and the PSS with enriched *Z*-isomer ratio are both higher in absence of DTT, and the PSS measurement shows slightly less activity compared to the isolated *E*-isomer. However, so far it was not possible to perform the CK1 δ assays without GSH.

Based on the evidence for the formation of the hydrazine 31 in presence of DTT, we co-crystallized the complex of compound 2 and p38 α without adding DTT. In this structure we observed compound 2 in the *E*-configuration as the major population (see ESI Fig. S50c[†]). However, even in this case a

small amount of the molecule was reduced (presumably because of trace amounts of remaining DTT or the protein itself being responsible for the reduction).

In contrast to our observation of reduction of compound 2 during crystallization and within the *in vitro* kinase assay, compound 3 was stable under conditions containing DTT. The redox properties of azobenzenes are significantly influenced by the electronic nature of the substituents. Concerning the reduction mechanism, electron poor azo compounds are generally more sensitive to reduction than electron rich compounds.^{50–52} This is consistent with our observation, that the 2-azo-thiazole 2 is rather electron poor compared to the 2-azo-imidazole 3, thus leading to a reduction of the thiazole compound 2. After successful co-crystallization of compound 3 with p38 α (Fig. 4), the diarylazo moiety was observed mainly in the *E*-configuration. In contrast to the previous example, the *E*-diarylazo moiety is still intact in 3, indicating enhanced susceptibility of thiazole 2 towards reduction, compared to imidazole 3. Furthermore, ¹H NMR and UV/vis investigations of imidazole 3 treated with DTT and GSH showed no indication for a reduction to the respective hydrazine.

CK1 δ . We also co-crystallized compound 2 and compound 3 together with CK1 δ (Fig. 6). Being aware of the high reduction susceptibility of compound 2, we removed DTT from the CK1 δ protein sample before setting up crystallization trials with this

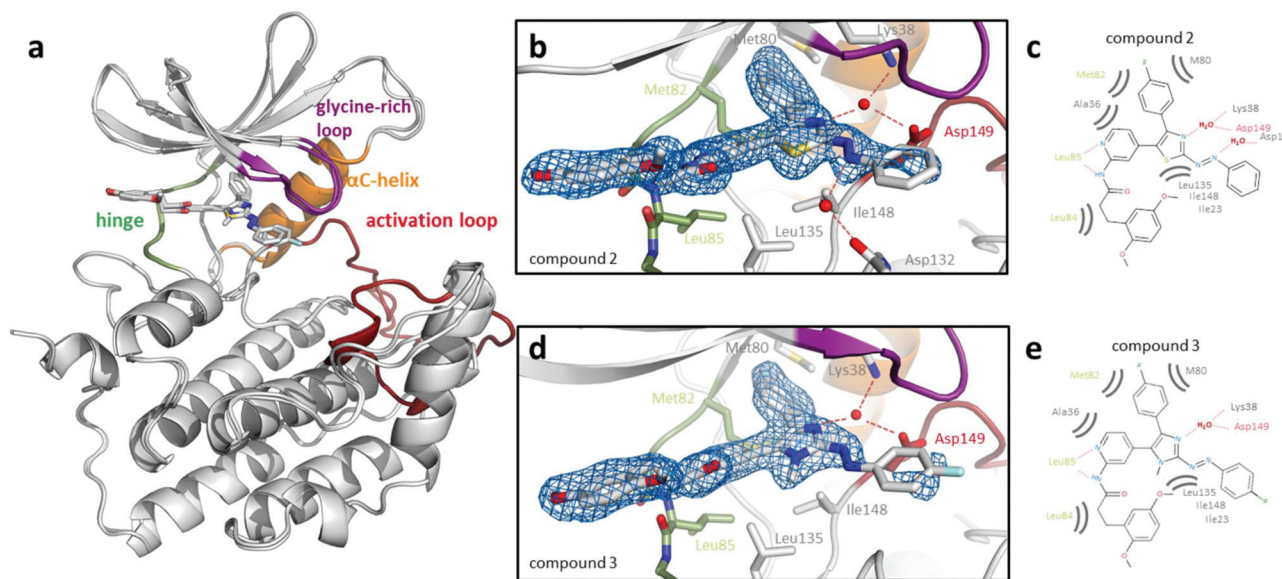


Fig. 6 Crystal structures of CK1 δ in complex with compounds 2 and 3. (a) Overview of the CK1 δ complex structures with compound 2 or 3 respectively. Important regions are colored: The hinge region in green, the glycine-rich loop in magenta, α C-helix in orange, and the activation loop in red. (b and d) Close-up of the binding pocket of both complex structures. The electron density (2Fo-Fc map) of the bound compounds is depicted as blue mesh with a contour level of 1 σ . (c and e) 2D representation of most important ligand-protein interactions. The 4,5-diaryl-imidazole scaffold binds to CK1 δ in a similar manner as it was for other compounds observed previously.²⁹ The diarylazo moiety was poorly resolved in the electron density suggesting that it adopts several conformations when bound to CK1 δ .

compound. Herein, the ligand-protein complex structures revealed that the 4,5-diaryl moieties of both compounds were binding in an identical way as observed in other inhibitors with this scaffold.²⁹ In both data sets, the azo moiety was present and could be well resolved by the electron density while the phenyl- (compound 2) or fluorophenyl- (compound 3) moieties were barely visible in the electron density maps. Hence, our data is indicating that the diarylazo moieties of both inhibitors are not adopting a stable conformation in CK1 δ . This flexibility could also explain why only minor photo-induced differences in the inhibition potencies of these compounds could be observed (Fig. 6).

Conclusions

Surprisingly, photoswitchable inhibitors based on diarylazo cores often exhibit small differences regarding biological activities of their *E*- and *Z*-isomers. In this study we aimed at the design, synthesis and characterization of photoswitchable kinase inhibitors. As the model system we used the well known vicinal diaryl scaffold (tear-drop binder^{53,54}) of p38 α - and CK1 δ -inhibitors. This basic structure was functionalized with photoswitchable diarylazo- respectively diazocine moieties in such a way that the corresponding *E*- and *Z*-isomers were predicted to exhibit different inhibitory activities. Much to our surprise, the diazocine-based compound 4 turned out not to inhibit these kinases, whereas compounds 2 and 3 were potent inhibitors with IC₅₀ values in the nanomolar range. However, in the course of our studies, we observed inconsis-

ent results for inhibitory activities of the respective photoswitchable *E/Z*-isomers of 2 and 3. Surprisingly, by solving a ligand-protein complex of 2 in p38 α by X-ray analysis we discovered the diarylazo unit being reduced by DTT to a hydrazine moiety yielding the new compound 31. Since reducing and stabilizing agents such as DTT and GSH are routinely used in biological assays our observation might generally pertain to other photoswitchable diarylazo inhibitors used in similar studies. Re-examination might be necessary in some cases. This is especially true since the higher susceptibility of the *Z* isomer toward reduction can simulate an apparent photoswitchable system and lead to wrong conclusions.

As a second limitation of the photoswitchable activity approach, we have observed a substantial ligand flexibility of compound 3 in CK1 δ and p38 α not translating into sufficient steric clashes of neither the *E*- nor the *Z*-ligand with the protein. Consequently, both isomers are able to bind to the active site, thus not yielding significant differences in inhibitory activities. In line with this observation and in addition to the flexibility of the ligand, a conformational adaption of the protein could also be responsible for an induced-fit type of binding levelling any designed *E/Z* affinity differences. With these results in mind, future investigations should carefully choose the position of the photoswitch within the core of the pharmacophore rather than being placed in a (flexible) side chain. Furthermore, compound concentration, PSS and respective *E/Z* half-lives in an aqueous medium play crucial roles for effective photoswitches in biological assays. Finally, the assay set-up under controlled light conditions turned out to be highly important to avoid artefacts.

Consideration of these pitfalls and limitations in photo-switchable inhibitor design might improve efficiencies and reduce the probability of misinterpretations.

Notes

Compound	PDB code p38 α	PDB code CK1 δ
2	6HWU	6HMR
3	6HWV	6HMP
31	6HWT	—

Authors will release the atomic coordinates and experimental data upon article publication. Co-crystallization of compounds 2, 3, and 31 in p38 α ; compounds 2 and 3 in CK1 δ .

CCDC 1885848† contains the supplementary crystallographic data for compound 13.

Conflicts of interest

There are no conflicts to declare.

Acknowledgements

The authors from Kiel university acknowledge financial support by the Deutsche Forschungsgesellschaft (DFG) within the Sonderforschungsbereich 677, "Function by Switching". Chiara Ianes is financially supported by a grant of the medical faculty of Ulm University ("Bausteinprogramm") awarded to Joachim Bischof. Work in the lab of Uwe Knippschild was supported by the DFG (KN356/6-1, and SFB 1149, project B04). Daniel Rauh is thankful for support from the German Federal Ministry for Education and Research (NGFNPlus and e:Med) (Grant No. BMBF 01GS08104, 01ZX1303C), the Deutsche Forschungsgemeinschaft (DFG) and the German federal state North Rhine Westphalia (NRW) and the European Union (European Regional Development Fund: Investing In Your Future) (EFRE-800400). The crystallographic experiments leading to these results have received funding from the European Community's Seventh Framework Programme (FP7/2007-2013) under grant agreement No. 283570 (BioStruct-X). CK1 δ crystals were grown in the Cologne Crystallization facility (<http://C2f.uni-koeln.de/>). We thank the staff at the Swiss Light Source, Paul Scherrer Institute, Villigen, Switzerland for their support during data collection. We gratefully acknowledge the help of Dr Dieter Schollmeyer, University of Mainz, Institute for Organic Chemistry, Germany, for X-ray analysis of compound 13.

Notes and references

- V. Balzani, A. Credi, F. M. Raymo and J. F. Stoddart, *Angew. Chem., Int. Ed.*, 2000, **39**, 3348–3391.
- W. Browne and B. L. Feringa, *Nat. Nanotechnol.*, 2006, **1**, 25–35.
- S. Kassem, T. van Leeuwen, A. S. Lubbe, M. R. Wilson, B. L. Feringa and D. A. Leigh, *Chem. Soc. Rev.*, 2017, **46**, 2592–2621.
- K. Matsuda and M. Irie, *J. Photochem. Photobiol., C*, 2004, **5**, 169–182.
- T.-T. Nguyen, D. Türp, M. Wagner and K. Müllen, *Angew. Chem., Int. Ed.*, 2013, **52**, 669–673.
- G. Mayer and A. Heckel, *Angew. Chem., Int. Ed.*, 2006, **45**, 4900–4921.
- A. A. Beharry and G. A. Woolley, *Chem. Soc. Rev.*, 2011, **40**, 4422–4437.
- M. M. Lerch, M. J. Hansen, G. M. van Dam, W. Szymanski and B. L. Feringa, *Angew. Chem., Int. Ed.*, 2016, **55**, 10978.
- K. Hüll, J. Morstein and D. Trauner, *Chem. Rev.*, 2018, **118**, 10710–10747.
- W. Szymanski, M. E. Ourailidou, W. A. Velema, F. J. Dekker and B. L. Feringa, *Chem. – Eur. J.*, 2015, **21**, 16517–16524.
- D. Vomasta, C. Högner, N. R. Branda and B. König, *Angew. Chem., Int. Ed.*, 2008, **47**, 7644–7647.
- R. Ferreira, J. R. Nilsson, C. Solano, J. Andrésson and M. Grötli, *Sci. Rep.*, 2015, **5**, 1–8.
- J. Kuil, L. T. M. van Wandelen, N. J. de Mol and R. M. J. Liskamp, *Bioorg. Med. Chem.*, 2008, **16**, 1393–1399.
- A. D. Abell, M. A. Jones, A. T. Neffe, S. G. Aitken, T. P. Cain, R. J. Payne, S. B. McNabb, J. M. Coxon, B. G. Stuart, D. Pearson, H. Y.-Y. Lee and J. D. Morton, *J. Med. Chem.*, 2007, **50**, 2916–2920.
- C. Falencyk, M. Schiedel, B. Karaman, T. Rumpf, N. Kuzmanovic, M. Grötli, W. Sippl, M. Jung and B. König, *Chem. Sci.*, 2014, **5**, 4794.
- M. J. Hansen, W. A. Velema, G. de Bruin, H. S. Overkleeft, W. Szymanski and B. L. Feringa, *ChemBioChem*, 2014, **15**, 2053–2057.
- C. E. Weston, A. Krämer, F. Colin, Ö. Yildiz, M. G. J. Baud, F.-J. Meyer-Almes and M. J. Fuchter, *ACS Infect. Dis.*, 2017, **3**, 152–161.
- D. Wutz, D. Gluhacevic, A. Chakrabarti, K. Schmidtkunz, D. Robaa, F. Erdmann, C. Romier, W. Sippl, M. Jung and B. König, *Org. Biomol. Chem.*, 2017, **15**, 4882–4896.
- N. A. Smith, L.-M. Altmann, N. Wössner, E. Bauer, M. Jung and B. König, *J. Org. Chem.*, 2018, **83**, 7919–7927.
- D. Wilson, J. Li and N. Branda, *ChemMedChem*, 2017, **12**, 284–287.
- C. Schwab, A. J. DeMaggio, N. Ghoshal, L. I. Binder, J. Kuret and P. L. McGeer, *Neurobiol. Aging*, 2000, **21**, 503–510.
- G. Manning, D. B. Whyte, R. Martinez, T. Hunter and S. Sudarsanam, *Science*, 2002, **298**, 1912–1934.
- J. Zhang, P. L. Yang and N. S. Gray, *Nature*, 2009, **9**, 28–39.
- A. C. Dar and K. M. Shokat, *Annu. Rev. Biochem.*, 2011, **80**, 769–795.
- S. Gross, R. Rahal, N. Stransky, C. Lengauer and K. P. Hoeflich, *J. Clin. Invest.*, 2015, **125**, 1780–1789.

- 26 M. Huang, A. Shen, J. Ding and M. Geng, *Trends Pharmacol. Sci.*, 2014, **35**, 41–50.
- 27 C. Sun and R. Bernards, *Trends Biochem. Sci.*, 2014, **39**, 465–474.
- 28 S. Klaeger, S. Heinzlmeir, M. Willhelm, *et al.*, *Science*, 2017, **358**, 1–16.
- 29 J. Halekotte, L. Witt, C. Ianes, M. Krüger, M. Bührmann, D. Rauh, C. Pichlo, E. Brunstein, A. Luxenburger, U. Baumann, U. Knippschild, J. Bischof and C. Peifer, *molecules*, 2017, **22**, 522.
- 30 C. E. Weston, R. D. Richardson, P. R. Haycock, A. J. P. White and M. J. Fuchter, *J. Am. Chem. Soc.*, 2014, **136**, 11878–11881.
- 31 J. Otsuki, K. Suwa, K. K. Sarker and J. Sinha, *J. Phys. Chem. A*, 2007, **111**, 1403–1409.
- 32 R. Siewertsen, H. Neumann, B. Buchheim-Stehn, R. Herges, C. Näther, F. Renth and F. Temps, *J. Am. Chem. Soc.*, 2009, **131**, 15594–15595.
- 33 S. Laufer and P. Koch, *Org. Biomol. Chem.*, 2008, **6**, 437–439.
- 34 S. Laufer and A. J. Liedtke, *Tetrahedron Lett.*, 2006, **47**, 7199–7203.
- 35 H. Beyer and G. Henseke, *Chem. Ber.*, 1950, **88**, 1233–1236.
- 36 B. Sahlmann, PhD Thesis, Christian-Albrechts-University Kiel, 2013.
- 37 M. Dommaschk, M. Peters, F. Gutzeit, C. Schütt, C. Näther, F. D. Sönnichsen, S. Tiwari, C. Riedel, S. Boretius and R. Herges, *J. Am. Chem. Soc.*, 2015, **137**, 7552–7555.
- 38 M. J. Hansen, M. M. Lerch, W. Szymanski and B. L. Feringa, *Angew. Chem., Int. Ed.*, 2016, **55**, 13514–13518.
- 39 T. Wendler, C. Schütt, C. Näther and R. Herges, *J. Org. Chem.*, 2012, **77**, 3284–3287.
- 40 J. Roger and H. Doucet, *Tetrahedron*, 2009, **65**, 9772–9781.
- 41 M. Hammerich, C. Schütt, C. Stähler, P. Lentos, F. Röhricht, R. Höppner and R. Herges, *J. Am. Chem. Soc.*, 2016, **138**, 13111–13114.
- 42 H. Kim, I. Yang, R. S. Patil, S. Kang, J. Lee, H. Choi, M.-S. Kim, S.-J. Nam and H. Kang, *J. Nat. Prod.*, 2014, **77**, 2716–2719.
- 43 D. K. Joshi, M. J. Mitchell, D. Bruce, A. J. Lough and H. Yan, *Tetrahedron*, 2012, **68**, 8670–8676.
- 44 J. Calbo, C. E. Weston, A. J. P. White, H. S. Rzepa, J. Contreras-García and M. J. Fuchter, *J. Am. Chem. Soc.*, 2017, **139**, 1261–1274.
- 45 S. Devi, M. Saraswat, S. Grewal and S. Venkataramani, *J. Org. Chem.*, 2018, **83**, 4307–4322.
- 46 W. G. Levine, *Drug Metab. Rev.*, 1991, **23**, 253–309.
- 47 A. A. Beharry, L. Wong, V. Tropepe and G. A. Woolley, *Angew. Chem., Int. Ed.*, 2011, **50**, 1325–1327.
- 48 L. Stricker, M. Böckmann, T. M. Kirse, N. L. Doltsinis and B. J. Ravoo, *Chem. – Eur. J.*, 2018, **24**, 8639.
- 49 C. Renner and L. Moroder, *ChemBioChem*, 2006, **7**, 868–878.
- 50 S. Zbaida, *Drug Metab. Rev.*, 1995, **27**, 497–516.
- 51 C. Boulègue, M. Löweneck, C. Renner and L. Moroder, *ChemBioChem*, 2007, **8**, 591–594.
- 52 W. A. Velema, W. Szymanski and B. L. Feringa, *J. Am. Chem. Soc.*, 2014, **136**, 2178–2191.
- 53 B. A. Thaher, M. Arnsmann, F. Totzke, J. E. Ehlert, M. H. G. Kubbutat, C. Schächtele, M. O. Zimmermann, P. Koch, F. M. Boeckler and S. A. Laufer, *J. Med. Chem.*, 2012, **55**, 961–965.
- 54 A. Freitag and S. A. Laufer, *Nachr. Chem.*, 2015, **63**, 420–425.